Epitaxial growth and magnetic properties of Mn5(SixGe1-x)3 thin films

Sueyeong Kang, Matthieu Petit, Vasile Heresanu, Alexandre Altié, Thomas Beaujard, Ganaël Bon, Oscar Cespedes, Brian Hickey, Lisa Michez

Thin Solid Films 797 (2024) 140338

Contents lists available at ScienceDirect

Thin Solid Films

journal homepage: www.elsevier.com/locate/tsf

Epitaxial growth and magnetic properties of $Mn_5(Si_xGe_{1-x})_3$ thin films

Sueyeong Kang [a], Matthieu Petit [a,*], Vasile Heresanu [a], Alexandre Altié [a], Thomas Beaujard [b], Ganaël Bon [b], Oscar Cespedes [c], Brian Hickey [c], Lisa Michez [a]

[a] Aix Marseille Univ, CNRS, CINaM, AMUTECH, Marseille, 13288, France
[b] Aix Marseille Univ, Polytech Marseille, Department of Materials Science and Engineering, Marseille, 13288, France
[c] School of Physics and Astronomy, University of Leeds, Leeds, LS2 9JT, United Kingdom

ARTICLE INFO

Keywords:
Molecular beam epitaxy
Epitaxial growth
Manganese silicide germanide
Manganese germanide
Manganese silicide
Ferromagnetism
Antiferromagnetism

ABSTRACT

Structural and magnetic properties of $Mn_5(Si_xGe_{1-x})_3$ thin films were investigated. Ferromagnetic Mn_5Ge_3 and anti-ferromagnetic Mn_5Si_3 thin films have been synthesized and characterized as these compounds exhibit interesting features for the development of spintronics. Here, $Mn_5(Si_xGe_{1-x})_3$ thin films were grown on Ge(111) substrates by co-deposition using molecular beam epitaxy. Crystalline thin films can be produced with controlled Si concentrations ranging from 0 to 1. The thin films were relaxed by dislocations at the interface with the substrate. A lattice parameter variation was observed as the Si content increased, which is comparable to previous works done in bulk. Reflection high-energy electron diffraction diagrams and X-ray diffraction profiles showed that lattice parameters a and c are shrinking and that the surface roughness and crystallinity degrade as the Si amount increases. Magnetometric measurements revealed a ferromagnetic behavior for all Si concentrations. The measured average ferromagnetic moment per manganese atom decreased from 2.33 to 0.05 μ_B/Mn atom. No ferro to anti-ferromagnetic transition was observed contrary to the bulk $Mn_5(Si_xGe_{1-x})_3$ compound.

1. Introduction

Manganese silicide and manganese germanide compounds have the advantage of being rare earth-free alloys. They are drawing great attention, both in the field of spintronics and magnetocaloric materials. Magnetic cooling, using the magnetocaloric effect (MCE), has a high potential as a solution for efficient thermal management. Manganite materials such as Mn-T-X (T = Ni, Co and X = Si, Ge) exhibit interesting values of the adiabatic temperature change (ΔT_{ad}) and the magnetic entropy change (ΔS_M) and room temperature MCE are obtained for some of these compounds [1,2]. Among the manganite compounds, Mn_5Ge_3 and Mn_5Si_3 exhibit strong similarities but also fascinating differences, which are detailed in Table 1. Both compounds can be integrated as thin films on commonly used substrates such as silicon or germanium.

These two intermetallic alloys have a hexagonal $D8_8$-type structure: the Mn atoms occupy two different types of sites. The first type of site is a layer of manganese atoms only (named Mn_I in Wyckoff positions 4d (1/3, 2/3, 0)). The second type of site is a layer of manganese and germanium or silicon atoms (named Mn_{II} on positions 6 g (0.2358, 0, 1/4) plus column IV atoms on positions 6 g (0.5992, 0, 1/4)). These two layers alternate as illustrated in Fig. 1. The Mn_I atoms form a rectilinear chain of metallic bonds, whereas the Mn_{II} ones involve d^2s orbitals (sp^2 for Ge or Si atoms) [17].

The compounds can be grown by co-deposition epitaxy on Ge(111) substrate in the case of Mn_5Ge_3 and on Si(111) substrate in the case of Mn_5Si_3 [8,9]. In terms of magnetic properties, Mn_5Ge_3 exhibits ferromagnetic behavior with a Curie temperature (T_C) of 296 K, while Mn_5Si_3 is considered to have antiferromagnetic characteristics with two first-order transitions associated with structural changes in bulk: below 66 K, Mn_5Si_3 adopts a noncollinear antiferromagnetic phase (AF1). When the temperature exceeds this threshold, the first transition occurs, from AF1 to a collinear antiferromagnetic phase (AF2). The second transition takes place at T = 99 K, resulting in the transformation from the AF2 structure to a paramagnetic state [10–13]. The magnetocaloric properties of Mn_5Ge_3 and Mn_5Si_3 have also been studied. Mn_5Ge_3 presents a second order magnetic phase transition and a value of ΔS_M equal to 9.3 J kg^{-1} K^{-1} (5 T) [15]. Polycristalline Mn_5Si_3 exhibits an inverse magnetocaloric effect linked to the structural distortion and ΔS_M = 2 J kg^{-1} K^{-1} (3 T, 62 K) [16].

Considering the great differences in the magnetic behaviors of Mn_5Ge_3 and Mn_5Si_3, it is interesting to study the ternary alloys, denoted as $Mn_5(Si_xGe_{1-x})_3$, with a variable silicon concentration (x)

* Corresponding author.
E-mail address: matthieu.petit@univ-amu.fr (M. Petit).

https://doi.org/10.1016/j.tsf.2024.140338
Received 14 February 2024; Received in revised form 21 March 2024; Accepted 15 April 2024
Available online 20 April 2024

Table 1
Main properties of Mn_5Ge_3 and Mn_5Si_3 bulk compounds.

	Mn_5Ge_3	Mn_5Si_3
Structure	Hexagonal $D8_8$ (P63/mcm)	
Bulk lattice parameters (300 K)	a^{hex} = 7.18 Å c = 5.05 Å [3]	a^{hex} = 6.91 Å c = 4.81 Å [4]
Heat of formation (kJ (mol of at)$^{-1}$)	−18.4 [5]	−34.2 [6]
Epitaxial growth on:	Ge(111) [7,8]	Si(111) [9]
Epitaxial relationships	Mn_5Ge_3 (0001)//Ge(111) Mn_5Ge_3 $[\bar{2}110]$//Ge$[11\bar{2}]$	Mn_5Si_3 (0001)//Si(111) Mn_5Si_3 $[\bar{2}110]$//Si$[11\bar{2}]$
Lattice mismatch with Ge(111) substrate	−3.75%	+0.27%
Magnetic behaviors	Metallic ferromagnet (FM)	Metallic antiferromagnet (AFM)
Relevant temperatures (K)	T_C = 296 K [10]	Non-collinear AFM at T ≤ 66 K collinear AFM for 66 K ≤ T ≤ 99 K [11–13]
Relevant features	Uniaxial anisotropy along c-axis [14]	Topological Hall effect for T ≤ 66 K spontaneous Hall effect in epitaxial thin film for T ≤ 240 K [9]
Magnetocaloric properties	MCE effect, ΔS_M = 9.3 J kg^{-1} K^{-1} (5 T) [15]	Inverse MCE effect, ΔS_M = 2 J kg^{-1} K^{-1} (3 T) [16]

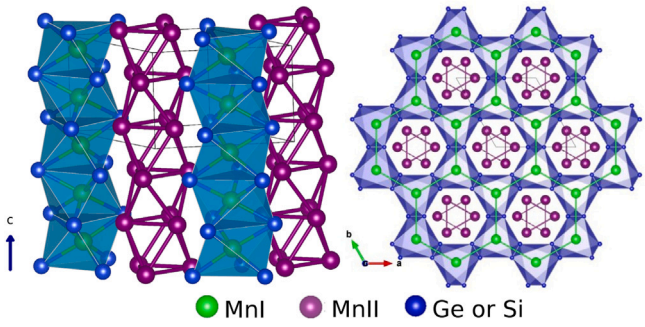

Fig. 1. Mn_5X_3 lattice structure with X = Ge or Si. Mn_I atoms form layers of only Mn atoms perpendicular to the c axis. Some of the Mn_{II} atoms create octahedra chains parallel to the c axis. (The diagrams presented here were generated using Vesta software [24].)

in the range [0; 1]. Previous research has predominantly dealt with either bulk $Mn_5(Si_xGe_{1-x})_3$ single crystals or polycrystalline samples, synthesized from melted pure Mn, Ge, and Si flakes, subsequently annealed several days at temperatures around 900–1120 K for homogenization [18,19]. A comprehensive investigation into the structural, magnetic, and electrical properties of the bulk $Mn_5(Si_xGe_{1-x})_3$ alloys has been conducted. All bulk $Mn_5(Si_xGe_{1-x})_3$ compounds exhibit the same hexagonal $D8_8$ crystalline structure belonging to the space group P63/mcm at 300 K. The lattice parameters of the unit cell decrease with the increase of x. Berche et al. show the existence of a gradual kinetic phase separation phenomenon, leading to the transformation of the $Mn_5(Si_xGe_{1-x})_3$ solid solution into the separated Mn_5Ge_3 and Mn_5Si_3, particularly with increasing annealing temperature [19]. The $Mn_5(Si_xGe_{1-x})_3$ alloys exhibit a macroscopic ferromagnetic behavior within the x range of 0 to 0.75, with T_C varying from 296 K to 151 K. The mean ferromagnetic moment per manganese atoms μ_F decreases as x increases. At a Si concentration of approximately x = 0.8, the magnetic behavior tips from ferromagnetic to antiferromagnetic order, with total magnetization nearing zero at x = 0.85. Resistivity measurements conducted over a temperature range of [4; 30] K also confirm this transition [18,20–22]. Theoretical calculations regarding Si substitution in Mn_5Ge_3 indicate that the variation in the magnetic moments of the Mn_I atoms is slightly greater than that of the Mn_{II} atoms. This variation could be attributed to the modifications in the Mn-Mn distances with the Si content [23].

In this article, we have employed a combination of techniques, including *in situ* reflection high-energy electron diffraction (RHEED), X-ray diffraction (XRD), atomic force microscopy (AFM), and high-resolution transmission electronic microscopy (HR-TEM), to investigate the growth of $Mn_5(Si_xGe_{1-x})_3$ thin films on Ge(111) substrates via the molecular beam epitaxy (MBE) method. Additionally, the magnetic properties of the synthesized films were also characterized using a vibrating sample magnetometer (VSM) and a superconducting quantum interference device (SQUID). The purpose of our work is to provide a comparative analysis of $Mn_5(Si_xGe_{1-x})_3$ films in relation to the previous study on bulk with a view to their integration into a device heterostructure [18,20–22].

2. Experiments details

30 nm thick $Mn_5(Si_xGe_{1-x})_3$ thin films were prepared through the co-deposition of germanium, manganese, and silicon onto Ge(111) substrates using MBE. In the MBE setup with a base pressure better than 2×10^{-7} Pa, germanium and manganese were evaporated from conventional Knudsen effusion cells, while silicon was evaporated from a sublimation source, all sourced from MBE-Komponenten. Notably, this MBE cluster is equipped with *in situ* RHEED, featuring a beam acceleration voltage of 30 kV, enabling real-time monitoring of the thin film growth process.

Before being introduced into the MBE chamber, Ge(111) substrates underwent chemical cleaning procedures [25]. Within the ultra-high vacuum (UHV) environment, the substrates were pre-annealed at 720 K for several hours followed by a flash-annealing step reaching up to 1020 K, aimed at eliminating any residual germanium oxide present on the substrate surface. Subsequently, a 60 nm thick germanium buffer layer was grown over the Ge(111) substrate at 720 K, followed by annealing at 800 K to produce a high-quality germanium surface with a distinct c(2 × 4) reconstruction, which was confirmed by *in situ* RHEED observations.

Deposition rates of Mn, Ge, and Si were carefully calibrated using a quartz microbalance. The actual co-deposition onto the Ge buffer occurred simultaneously under UHV conditions maintained at 10^{-7} Pa and at a substrate temperature of 373 K. The presence of $Mn_5(Si_xGe_{1-x})_3$ layers was verified through the observation of the typical Mn_5Ge_3 $(\sqrt{3} \times \sqrt{3})R30°$ RHEED pattern [25,26]. No subsequent annealing was performed on the thin films after the co-deposition in order to avoid inter-diffusion between the film and the substrate as much as possible.

To assess crystalline orientation and quality of the thin films, 2-dimensional X-ray diffraction (2D-XRD) patterns were acquired using a high brilliancy rotating anode Rigaku RU-200BH, equipped with an image plate detector Mar345 and operating with the non-monochromatic Cu Kα radiation (λ = 1.54180 Å). During measurement, the angle between the X-ray beam and the sample's surface varies continuously from 5 to 35 degrees. The maximum measurable 2θ is 65 degrees. 1D diffraction patterns (intensity versus 2θ) are obtained by plotting the intensity, integrated over a constant radial distance, versus the radial distance. The quality of interfaces and their correlation with epitaxial growth on the Ge(111) surface was investigated through HR-TEM measurements. These measurements were performed using a JEM-2100F (JEOL) instrument, operating at an accelerating voltage of 200 kV and a spatial resolution of 2.3 Å. Prior to HR-TEM analysis, samples underwent thinning via a precision ion polishing system (PIPS),

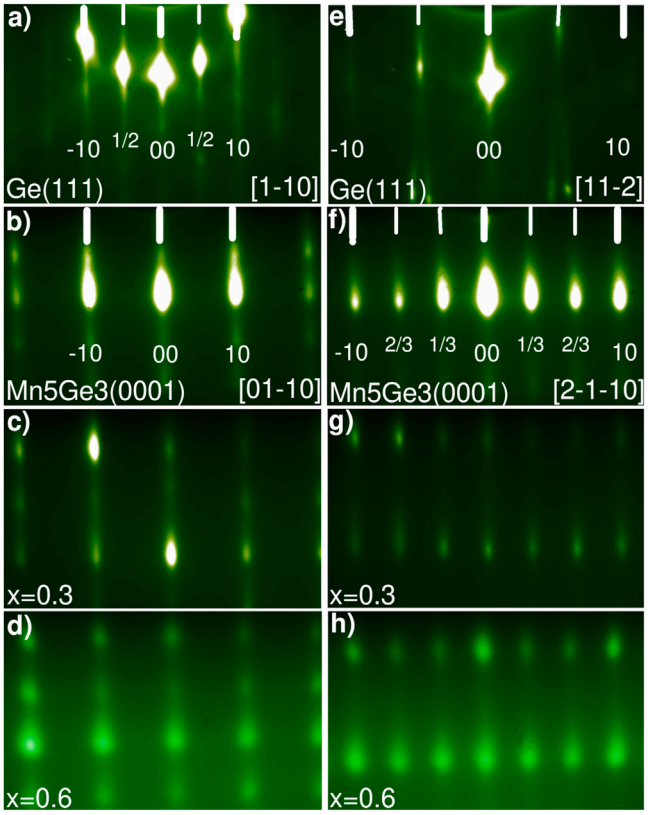

Fig. 2. RHEED patterns taken along the Ge(111)-[1$\bar{1}$0] (a)–(d) and Ge(111)-[11$\bar{2}$] (e)–(h) azimuths. The bulk 0 × 0 and 1 × 1 streaks are indicated with large white rods and the reconstructed streaks are marked with small white rods. Patterns (a) and (e): Ge(111)c(2 × 4) surface prior to the Ge, Si, and Mn co-deposition. Patterns (b)–(d) and (f)–(h): RHEED patterns taken at the end of the co-deposition of 30 nm thick $Mn_5(Si_xGe_{1-x})_3$ films with a silicon concentration x equal to 0 (i.e. Mn_5Ge_3 film, patterns (b) and (f)), x = 0.3 ($Mn_5(Si_{0.3}Ge_{0.7})_3$ film, patterns (c) and (g)), and x = 0.6 ($Mn_5(Si_{0.6}Ge_{0.4})_3$ film, patterns (d) and (h)). (The electron beam intensity is not constant throughout the RHEED screenshots).

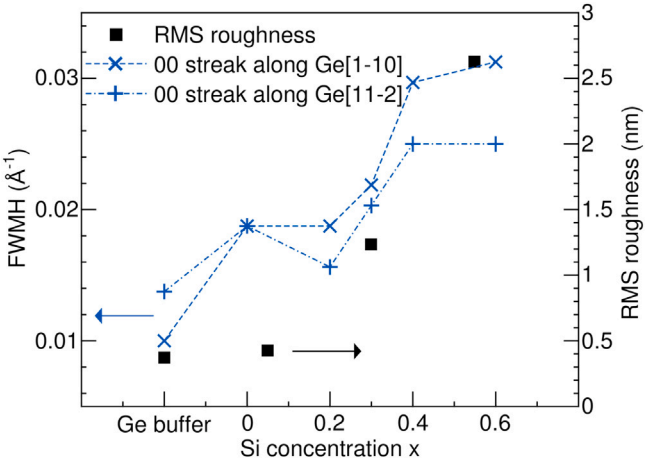

Fig. 3. left Y-axis: FWMH of the 00 streaks measured on RHEED patterns of the surface of Ge buffer and 30 nm thick $Mn_5(Si_xGe_{1-x})_3$ thin films, along the Ge[1$\bar{1}$0]-$Mn_5(Si_xGe_{1-x})_3$[01$\bar{1}$0] and Ge[11$\bar{2}$]-$Mn_5(Si_xGe_{1-x})_3$[2$\bar{1}$ $\bar{1}$0] azimuths. Right Y-axis: RMS roughness of Ge buffer and three $Mn_5(Si_xGe_{1-x})_3$ thin films (x = 0.05, 0.3, and 0.55) measured by AFM.

allowing the acquisition of cross-sectional images. Surface topographies were obtained by AFM with a Nanoscope IIIA Multimode from Digital instruments on a 2 × 2 μm^2 area. The magnetic properties of the thin films were probed using a Maglab 9 T VSM from Oxford instruments and an MPMSXL SQUID magnetometer from Quantum Design.

3. Results and discussion

3.1. Structure of the $Mn_5(Si_xGe_{1-x})_3$ thin films

A series of $Mn_5(Si_xGe_{1-x})_3$ samples with a variation of x from 0 to 1 were grown on Ge(111) substrates by co-deposition with a careful adjustment of the values of the Ge, Si, and Mn flux. Epitaxial growth was performed by simultaneously opening the shutters of Ge, Si, and Mn cells. The RHEED patterns of the initial Ge(111) surface exhibited a well defined c(2 × 4) reconstruction (Fig. 2(a) and (e)), indicating a clean and long scale ordered surface.

The identical Mn_5Ge_3 characteristic ($\sqrt{3} \times \sqrt{3}$)R30° reconstruction patterns were observed through RHEED analysis conducted on $Mn_5(Si_xGe_{1-x})_3$ thin films, indicating the fact that the surface structure remained unchanged regardless of the Si concentration (Fig. 2(b)–(d) and (f)–(h)). However, as the Si substitution increased, RHEED patterns became spottier and the streaks got more blurred. To quantify this observation, Fig. 3 displays the evolution of the full width at half maximum (FWHM) of the 00 RHEED streaks over x. The FWHM values of each 00 streak were obtained by plotting an intensity profile perpendicular to the streaks on RHEED patterns recorded at the end of the co-deposition process for 30 nm thick $Mn_5(Si_xGe_{1-x})_3$ films. This parameter is mostly linked to the vertical amplitude of roughness of the given surface [27,28]. Additionally, the root mean square (RMS) roughnesses were evaluated by AFM on some of these films in agreement with RHEED observations.

To assess the crystallinity of the $Mn_5(Si_xGe_{1-x})_3$ films, 2D-XRD patterns were recorded for various Si concentrations. Fig. 4(a) shows a representative 2D diffraction pattern of a $Mn_5(Si_{0.1}Ge_{0.9})_3$ film.

Fig. 4(b) presents the equivalent 1D diffraction patterns, integrated intensity versus radius, of the 2D patterns of thin films with Si concentrations ranging from x = 0 to 1. The two intense peaks at 2θ = 27.30° and 53.73° are originated from the Ge substrate and correspond to Ge(111) and Ge(311) planes, respectively. Peaks around 2θ = 35.48°, 42.44° and 43.76° can be attributed to the (0002), (12$\bar{3}$1), and (11$\bar{2}$2) diffraction planes of $Mn_5(Si_xGe_{1-x})_3$, with a slight shift towards higher 2θ angles at increasing Si concentrations. Above x = 0.5 (Fig. 4(c)), a significant drop in the diffracted intensities as well as broadening of the peaks are observed in the 1D patterns. In addition, a new weak diffraction peak appears around 2θ = 37.5°, which corresponds to the powder diffraction of Mn_5Si_3(0002) reflection. This indicates the possible existence of Mn_5Si_3 crystalline grains in the films. As Si atoms are expected to substitute Ge atoms, the $Mn_5(Si_xGe_{1-x})_3$ films are predicted to crystallize in the hexagonal $D8_8$-type structure, with the lattice parameters falling between those of Mn_5Ge_3 and Mn_5Si_3 compounds. Since phase separation has been demonstrated in bulk $Mn_5(Si_xGe_{1-x})_3$, the formation of Mn_5Si_3 grains in the thin films can be favorable during the co-deposition at higher Si concentrations rather than forming a $Mn_5(Si_xGe_{1-x})_3$ film with a sole and homogeneous Si concentration. Moreover, previous work on the Mn_5Si_3 film on Si(111) demonstrated the need of a post-annealing step to form a crystalline Mn_5Si_3 film [9]. As no post-annealing was applied on our process, the crystallinity of the x = 1 sample is expected to be low. The decrease in the peak intensities and their broadening combined with the evolution of the RHEED patterns (Fig. 2) show that the crystalline quality of the $Mn_5(Si_xGe_{1-x})_3$ films dropped with the increase of x. Regarding the peak positions, an increase in Si substitution x leads to a peak shift towards a higher 2θ angle, indicating a shrinkage of the lattice parameters. The lattice parameters a and c were calculated based on two diffraction reflections, (0002) and (12$\bar{3}$1). Fig. 5(a) and (d) present the evolution of both a and c, as well as the ratio c/a, in relation to Si concentrations below 0.6. Indeed, the accuracy of determining

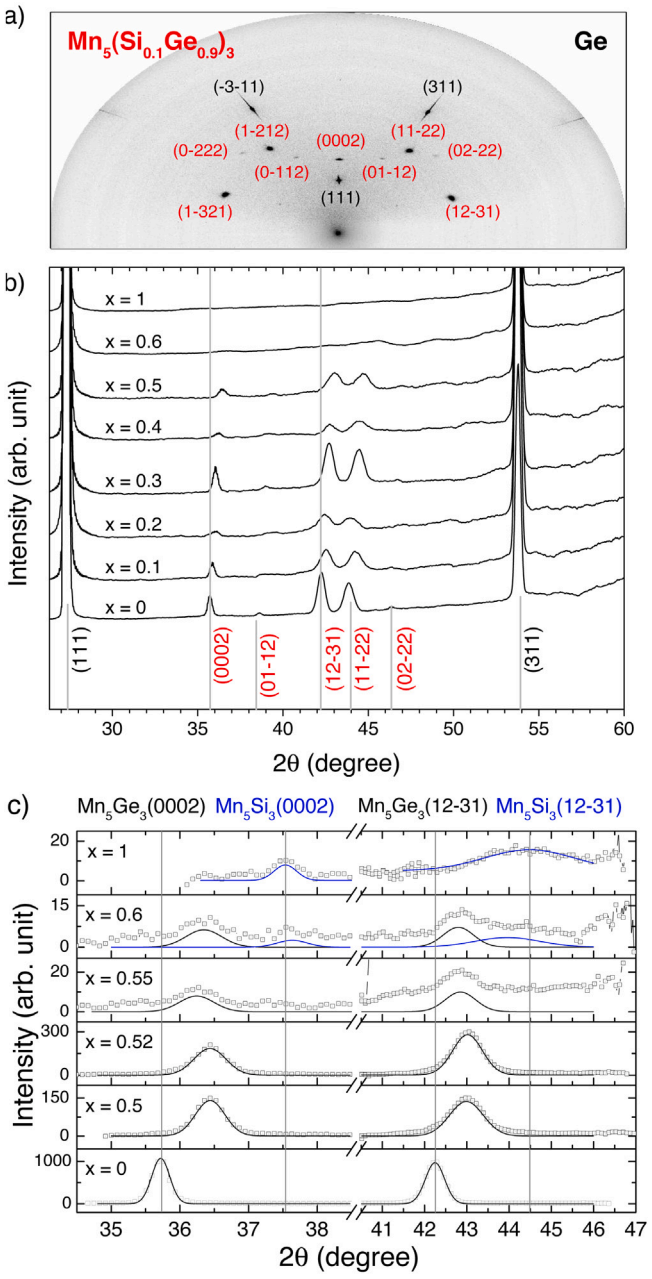

Fig. 4. X-ray diffraction data of $Mn_5(Si_xGe_{1-x})_3$ samples. (a) A typical 2D-XRD pattern obtained for $Mn_5(Si_{0.1}Ge_{0.9})_3$, with each spot corresponding to the diffraction angles of the labeled planes. (b) XRD profiles generated from the integrated intensities for equal radial distance, i.e. for equal 2θ angle, of the 2D-XRD patterns of $Mn_5(Si_xGe_{1-x})_3$ samples with Si concentration x = 0 to 1. As these profiles are an integration of 2D patterns, they contain both symmetric and asymmetric diffraction peaks. The lattice planes associated with the deflection angles of Germanium and $Mn_5(Si_xGe_{1-x})_3$ are marked in black and red, respectively. (c) XRD profiles focusing on high Silicon content thin films, ranging from x = 0.5 to x = 1. Symbols indicate the experimental data points and solid lines represent Gaussian fits of the data. Powder diffraction angles for Mn_5Ge_3 and Mn_5Si_3 are indicated by gray lines.

parameters is affected by the low intensity of the diffraction peaks above x = 0.6. However, both a and c values decrease linearly as x increases within the accessible concentration range and align well with those of the bulk alloys found in literature, as shown in Fig. 5(b), (c), and (e) [18,20,22].

Fig. 6(a) displays a cross-sectional HR-TEM image of a 30 nm thick $Mn_5(Si_{0.2}Ge_{0.8})_3$ thin film on a Ge(111) substrate. The surface of the film exhibits some roughness. Fig. 6(b) is focused on the interface between the thin film and the substrate and unveils a crystalline film epitaxially grown on the Ge(111) substrate. The identified zone axis of the film is [01$\bar{1}$0] and the [0001] axis is parallel to the Ge[111] in accordance with the epitaxial relationships established using RHEED and XRD techniques. The lattice parameter calculated from the TEM image is 7.18 Å, which is consistent with the value found by XRD (7.19 Å).

3.2. Mismatch accommodation

The fact that the lattice parameters a and c of the $Mn_5(Si_xGe_{1-x})_3$ films are close to those in the bulk (Fig. 5) means that the thin films are relaxed. To get a better insight into the relaxation process, we recorded a movie of the RHEED diagram during the first 26 Å of the co-deposition growth in the Ge(111)-[1$\bar{1}$0] azimuth. From this movie, we extracted the evolution of the in-plane lattice parameter of the growing film and the evolution of the intensity of the 00 streak (I_{00}) and of the background intensity (I_{bckg}) over the thickness of the film. The in-plane lattice parameter was calculated by converting the spacing of the RHEED streaks into a real space distance. The background intensity was measured at a location between the 00 and 01 streaks. Fig. 7(a) displays the evolution of the in-plane parameter over the whole first 26 Å of the co-deposition of a $Mn_5(Si_{0.3}Ge_{0.7})_3$ thin film as an illustration. It is representative of the other concentrations.

Starting at 4.00 Å, this in-plane parameter value at the given azimuth corresponds to the lattice parameter of the Ge(111) surface, $a_{Ge}/\sqrt{2}$. Between 1 and 12 Å of thickness, the value underwent an abrupt change. The longer error bars reflect an increase in the blurring of the RHEED stripes. Then, it stabilized at 4.13 Å around a film thickness of 12 Å. Along the observed $Mn_5(Si_xGe_{1-x})_3$ (0001)-[01$\bar{1}$0] azimuth, the spacing of the RHEED streaks corresponds to $a_{Mn_5(Si_xGe_{1-x})_3}/\sqrt{3}$ which gives $a_{Mn_5(Si_{0.3}Ge_{0.7})_3}$ = 7.15 Å, in good agreement with the XRD results, 7.14 Å (Fig. 5(a)). From this evolution of the in-plane parameter, we concluded that the thin film had relaxed in this short span of thickness. Looking more precisely in the range of 0 to 10 Å of co-deposition (Fig. 7(b)), the change in the in-plane parameter consisted of a slight decrease followed by an increase up to 4.40 Å again followed by a final decrease to the steady state value of 4.13 Å. Furthermore, the RHEED intensities exhibited abrupt fluctuations, particularly when I_{bckg} increased before decreasing and becoming stable. This increase is indicative of a transient disordering of the surface at the given co-deposition thickness. Closer examination of the TEM image (Fig. 6(b)) showed that the interface exhibited some stacking faults (marked by the dotted white square on the right side of Fig. 6(b)) and misfit dislocations (marked by the dotted white square on the left side of Fig. 6(b)). The formation of these defects explains the variation of the in-plane parameter measured by RHEED and the increase of the background intensity and has already been observed in the case of the growth of Mn_5Ge_3 thin films [29,30]. The accommodation of the lattice mismatch between the $Mn_5(Si_xGe_{1-x})_3$ films and the Ge(111) substrate seems to take place in a very thin layer of less than two $Mn_5(Si_xGe_{1-x})_3$ lattices thick. Note that after this transitory phase, I_{00} also reached a steady state, indicating that the growth front has stabilized.

3.3. Discussion of the $Mn_5(Si_xGe_{1-x})_3$ growth

The crystalline quality and the surface roughness of the $Mn_5(Si_xGe_{1-x})_3$ thin films degrade as x increases. This is not intuitive given the heats of formation and the lattice mismatches of the compounds (Table 1). On the basis of these parameters alone, Mn_5Si_3 appears to be the most favorable compound for epitaxial growth on Ge(111). Several other phenomena can be invoked to understand the evolution of $Mn_5(Si_xGe_{1-x})_3$ films with x. First, the low interface energy of the Mn_5Ge_3 /Ge(111) system ($\gamma_{Mn_5Ge_3/Ge(111)}$ = 0.53 J m^{-2}) plays a role in the epitaxial stability of the germanide phase on the Ge(111) substrate [31,32]. The growth of Mn_5Si_3 films on Si(111) requires a

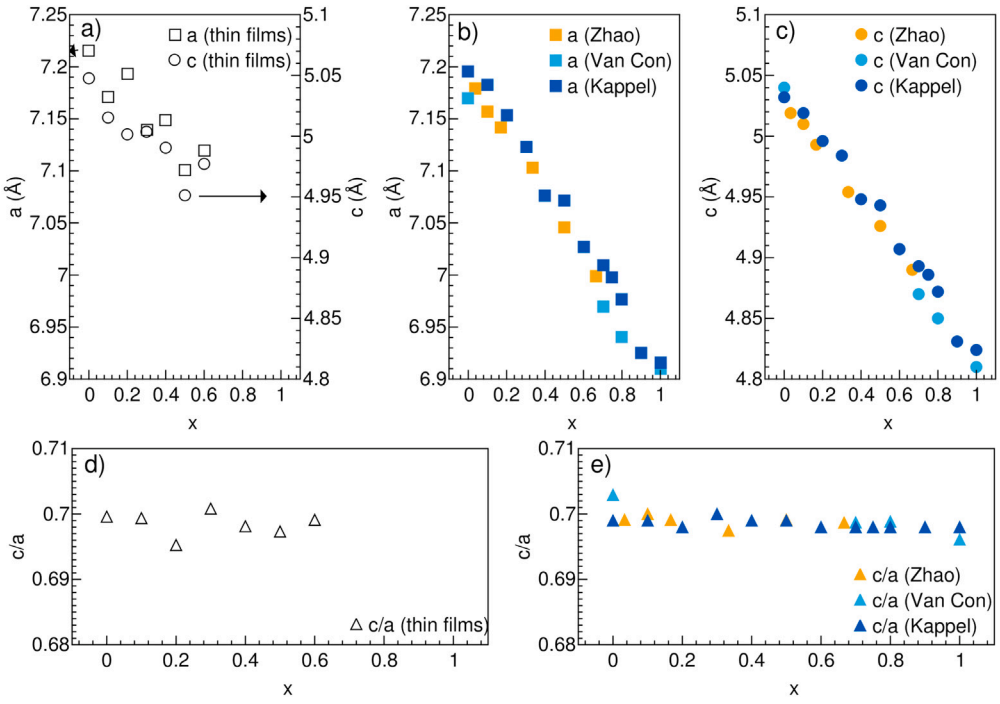

Fig. 5. (a) variation of the lattice parameters a and c of the $Mn_5(Si_xGe_{1-x})_3$ thin films versus the Si concentration x. (b) and (c) variation of the lattice parameters a and c respectively versus x in bulk samples, from Ref. [18,20,22]. (d) and (e) variation of the ratio c/a in the thin films and bulk compounds, respectively.

MnSi interfacial layer to reduce the surface energy and thus promote the crystallization of Mn_5Si_3 [9]. Although the surface energies of Ge(111) and Si(111) are not the same ($\gamma_{Ge(111)}$ = 1.30 J m^{-2}, $\gamma_{Si(111)}$ = 1.74 J m^{-2}), the interfacial energy of the $Mn_5(Si_xGe_{1-x})_3$ /Ge(111) system may not offer favorable conditions for the film nucleation as x increases [33]. Next, the initial stages of Mn atom adsorption on the Ge(111) surface are believed to be important for the crystal growth of Mn_5Ge_3 films. An impinging Mn atom first takes up position on a Ge adatom site (in a T_4 site) before shifting to a neighboring H_3 adsorption site [26]. Two out of three H_3 sites are occupied by Mn atoms. These well-defined Mn positions initiate the Mn_I rectilinear chains of the Mn_5Ge_3 lattice with the c-axis perpendicular to the substrate surface [29]. In the case of $Mn_5(Si_xGe_{1-x})_3$, Si atoms are expected to substitute for Ge atoms, but lower surface mobility of Si atoms than Ge atoms on Ge(111) surface and potential competition for adsorption sites between silicon and manganese atoms may be detrimental to the further ordering of the $Mn_5(Si_xGe_{1-x})_3$ layer [34,35]. Finally, although co-deposition (and not solid phase epitaxy) is considered in this article, diffusion phenomena may play a significant role in the formation and crystallization of the $Mn_5(Si_xGe_{1-x})_3$ films. Mn diffusion has been proven to be vacancy mediated and quite fast during phase formation in Mn_5Ge_3 [36,37], and the chains of vacancies created parallel to the Mn_I rectilinear chains above the unoccupied H_3 sites can provide preferential diffusion pathways. Moreover, Mn_5Ge_3 thin films can be synthesized on Ge(111) substrates with good crystallinity without an annealing step after co-deposition, whereas crystalline Mn_5Si_3 films are more difficult to produce on Si(111) substrates, as they require annealing at 500 K [8,9]. Noting also that the $Mn_5(Si_xGe_{1-x})_3$ lattice shrinks with increasing x, which may slow diffusion through the free volumes available in the lattice, the formation of $Mn_5(Si_xGe_{1-x})_3$ crystalline films is hampered by increasing Si concentration.

3.4. SQUID-VSM magnetometry

The magnetic behavior of $Mn_5(Si_xGe_{1-x})_3$ samples was measured using VSM (x = 0, 0.2, 0.4, and 0.6) and SQUID (x = 1). Magnetic hysteresis loops were acquired by VSM up to a magnetic field of 1 T, covering temperatures ranging from 20 K to 290 K with 10 K intervals. The raw data were processed to minimize experimental contributions: the magnetic moments of germanium substrates were subtracted. For x = 1 sample, magnetization versus temperature data were collected at a magnetic field of 1 T within the temperature range of 2 K to 400 K using SQUID, due to the signal intensity being too weak for a VSM measurement. For comparison of the magnetic moment recorded at 1 T (M_{1T}) with respect to silicon content, the measured M_{1T} were normalized to the volume of the samples and are plotted on Fig. 8(a). At 1 T, the saturation value is reached for the magnetization for the samples with low values of x ($M_{1T} = M_{sat}$).

Overall, magnetizations decrease with increasing temperature, corresponding to the demagnetization process of ferromagnetic materials. Mn_5Si_3 on Ge(111) shows an unusual M-T curve with *a piori* ferromagnetic characteristics. The T_C of samples with x = 0 to 0.6 were determined by fitting the M-T curves using a phenomenological model that obeys the Bloch power law at low temperature and reproduces the critical behavior near T_C [38]:

$$M(T) = M(0)\left[1 - s\left(\frac{T}{T_C}\right)^{\frac{3}{2}} - (1-s)\left(\frac{T}{T_C}\right)^{p}\right]^{\frac{1}{3}} \quad (1)$$

where $s \geq 0$ and $p \geq \frac{3}{2}$ are fitting parameters. For the x = 1 and even for x = 0.6 samples, the shapes of the M-T curves are not well described by the model as they do not exhibit a sharp transition around T_C. Yasasun et al. also observed an indistinct and broad transition near T_C in the M-T curve of their Mn_5Si_3 dominated sample [39]. The magnetic transition temperature of the Mn_5Si_3 sample was therefore evaluated using the derivative $\frac{dM}{dT}$ of the SQUID experimental data. All the T_C are reported on Table 2 and decrease as x increases.

The temperature of the magnetic transition of Mn_5Si_3 on Ge(111) substrate is different from the temperature found on Mn_5Si_3 films grown on Si(111) substrate [9]. Additionally, the mean magnetic moments per Mn atoms, μ_{1T}, were calculated at 20 K for each Si content. Fig. 8(b) displays their evolution as the silicon content increases. μ_{1T} decreases with a drop at x ≥ 0.4. In particular, at x = 1 μ_{1T} is equal to 0.05 μ_B (M_{1T} = 19.4 emu cm^{-3}) at 20 K, which significantly contrasts

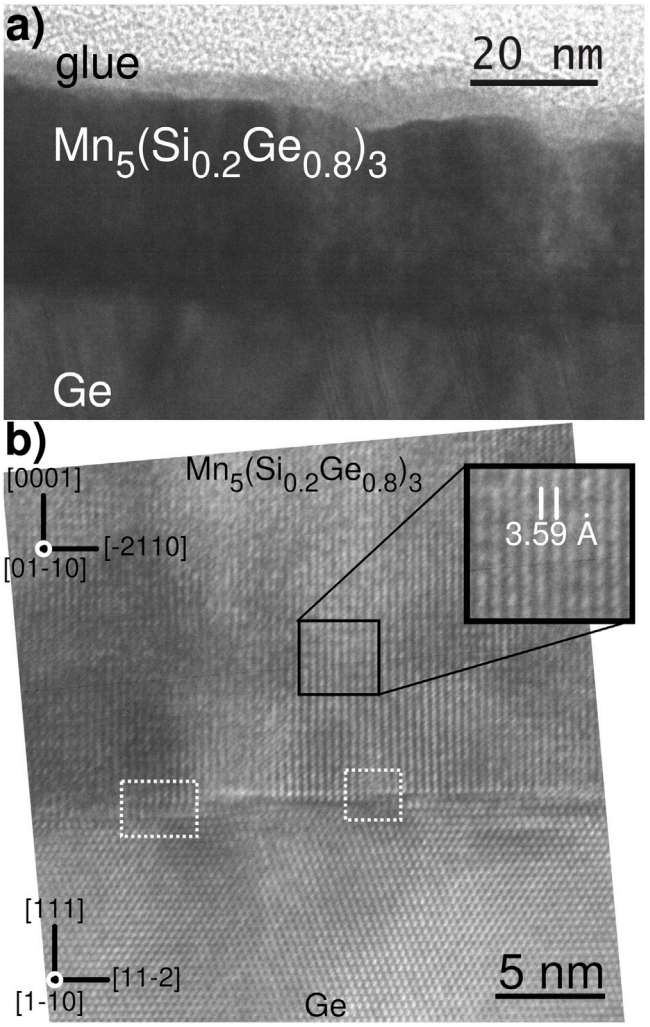

Fig. 6. (a) Transmission electron microscopy (TEM) image ~30 nm thick $Mn_5(Si_{0.2}Ge_{0.8})_3$ film. (b) High-resolution TEM image focused on the $Mn_5(Si_{0.2}Ge_{0.8})_3$/Ge(111) interface with a zoom (delimited with a black line) on the $Mn_5(Si_{0.2}Ge_{0.8})_3$ phase. The centers of interfacial dislocations are highlighted in white dotted squares.

Table 2
Curie temperatures (T_C) obtained by fitting the experimental data of Fig. 8 with the phenomenological model from Ref. [38]. R^2 is the correlation coefficient. T_C of x = 1 is obtained using SQUID ZFC-FC measurement.

Si content (x)	T_C (K)	R^2
x = 0.0	310	0.94
x = 0.2	311	0.97
x = 0.4	300	0.99
x = 0.6	296	0.70
x = 1.0	285 ± 4	–

with the value at x = 0.6 where it reaches μ_{1T} = 0.92 μ_B (M_{1T} = 376.2 emu cm^{-3}) at 20 K. Comparing with the data from the bulk, the values of the mean magnetic moments per Mn atoms at saturation μ_{sat} also exhibit a decrease but the slope is not as high as in thin films [18,22,23]. A ferromagnetic to antiferromagnetic transition is not observed within the limits of silicon concentrations in thin films accessible with the current growth method, whereas in bulk samples, a transition is observed around x = 0.8 [18,20–22]. The slightly apparent ferromagnetic behavior of the Mn_5Si_3 film suggests the presence of very low crystalline $Mn_5(Si_xGe_{1-x})_3$ compounds at the interface with the Ge(111) substrate.

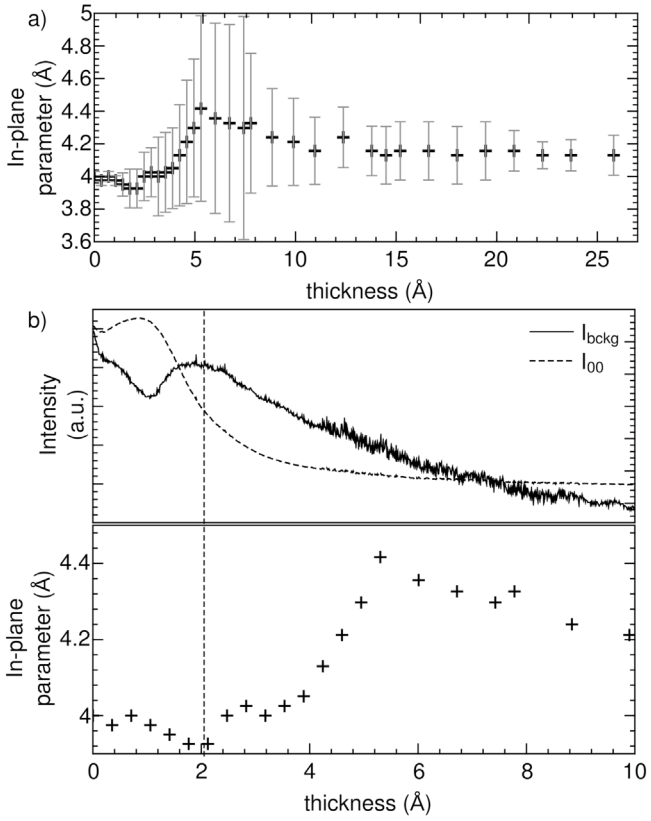

Fig. 7. (a) Tracking of the in-plane lattice parameter over the first 26 Å of the co-deposition obtained by measuring the RHEED streaks spacing in the Ge(111)-[1$\bar{1}$0] azimuth in the case of a $Mn_5(Si_{0.3}Ge_{0.7})_3$ thin film. (b) Zoom over the first 10 Å of the co-deposition of (top) $I_{(00)}$ the intensity of the 00 streak in the Ge(111)-[1$\bar{1}$0] azimuth and I_{bckg} the intensity of the background of the RHEED movie and (bottom) the in-plane parameter.

4. Conclusion

$Mn_5(Si_xGe_{1-x})_3$ thin films with x ranging from 0 to 1 were fabricated using MBE by co-deposition of Mn, Ge, and Si. Both structural and magnetic properties were investigated using RHEED, XRD, AFM, TEM, VSM, and SQUID. RHEED and XRD technics reveal that the lattice structure of thin films remains hexagonal $D8_8$ (P63/mcm) structure alike to Mn_5Ge_3 regardless of Si concentrations. By comparing the series of XRD integrated profiles and their peak shifts, we can conclude that both a and c parameters of hexagonal lattice shrink by increasing Si concentration. This result is in good agreement with the previous study on the bulk medium. The degradation of the crystalline and surface quality of the films is observed on higher Si concentration of x ≥ 0.5. Notably, Mn_5Si_3 (0002) and Mn_5Si_3 (12$\bar{3}$1) diffraction reflections were observed at this condition, indicating the occurrence of a possible phase separation. The analysis of the live-time RHEED patterns and TEM images shows that $Mn_5(Si_xGe_{1-x})_3$ thin films on Ge(111) are almost fully relaxed and that the relaxation takes place through dislocations in the interface. VSM and SQUID investigation display the decline of the overall magnetization as the temperature increases, confirming that $Mn_5(Si_xGe_{1-x})_3$ thin films present similar magnetic behavior as Mn_5Ge_3 thin film. Surprisingly, the Mn_5Si_3 film still exhibits a very weak ferromagnetic behavior. The mean magnetic moments per Mn atoms is affected by the increase of the Si content. However, the origin of this decrease is unclear and the substitution of Ge atoms by Si atoms as well as the increase in the crystalline disorder in the films may be an important factor. Further optimization of the growth process is required to synthesize crystalline $Mn_5(Si_xGe_{1-x})_3$ thin

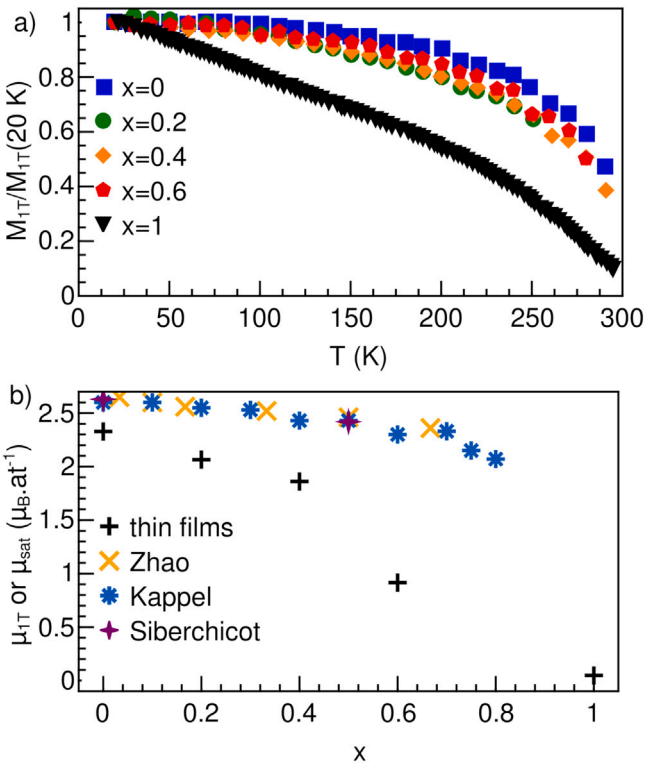

Fig. 8. (a) Temperature dependence of the magnetization (M_{1T}) of $Mn_5(Si_xGe_{1-x})_3$ samples obtained by VSM(x = 0 to 0.6) and SQUID(x = 1) recorded in a 1 T-field. (b) Evolution of the average saturation magnetic moment μ_{sat} at 20 K versus Si concentration x.
Source: Kappel, Siberchicot and Zhao are data from Ref. [18,22,23].

films over the entire Si concentration, and additional nuclear magnetic resonance (NMR) studies may provide a deeper understanding of the films' magnetic behavior.

CRediT authorship contribution statement

Sueyeong Kang: Conceptualization, Data curation, Formal analysis, Investigation, Methodology, Validation, Visualization, Writing – original draft. **Matthieu Petit:** Conceptualization, Data curation, Formal analysis, Investigation, Methodology, Project administration, Resources, Software, Supervision, Validation, Visualization, Writing – original draft, Writing – review & editing. **Vasile Heresanu:** Formal analysis. **Alexandre Altié:** Data curation. **Thomas Beaujard:** Data curation. **Ganaël Bon:** Data curation. **Oscar Cespedes:** Data curation. **Brian Hickey:** Data curation. **Lisa Michez:** Data curation, Formal analysis, Funding acquisition, Investigation, Project administration, Validation, Writing – review & editing.

Declaration of competing interest

The authors declare the following financial interests/personal relationships which may be considered as potential competing interests: Sueyeong Kang reports financial support was provided by European Cooperation in Science and Technology. If there are other authors, they declare that they have no known competing financial interests or personal relationships that could have appeared to influence the work reported in this paper.

Data availability

Data will be made available on request.

Acknowledgments

The authors would like to thank Cyril Coudreau and Christopher Genelot for technical support on the MBE cluster, and Alain Ranguis for the AFM images. This article is based upon work from COST-OPERA Action CA20116, supported by COST (European Cooperation in Science and Technology).

References

[1] A. Kitanovski, Energy applications of magnetocaloric materials, Adv. Energy Mater. 10 (2020) 1903741, http://dx.doi.org/10.1002/aenm.201903741.
[2] V. Chaudhary, X. Chen, R. Ramanujan, Iron and manganese based magnetocaloric materials for near room temperature thermal management, Prog. Mater. Sci. 100 (2019) 64–98, http://dx.doi.org/10.1016/j.pmatsci.2018.09.005.
[3] L. Castelliz, Beitrag zum ferromagnetismus von legierungen der übergangsmetalle mit elementen der B-gruppe, Int. J. Mater. Res. 46 (3) (1955) 198–203, http://dx.doi.org/10.1515/ijmr-1955-460308.
[4] B. Aronsson, A note on the compositions and crystal structures of MnB_2, Mn_3Si, Mn_5Si_3, and $FeSi_2$, Acta Chemica Scandinavica 14 (6) (1960) 1414–1418, http://dx.doi.org/10.3891/acta.chem.scand.14-1414.
[5] A. Berche, J. Tedenac, P. Jund, Thermodynamic modeling of the germanium–manganese system, Intermetallics 47 (2014) 23–30, http://dx.doi.org/10.1016/j.intermet.2013.12.009.
[6] A. Berche, J.-C. Tédenac, P. Jund, First-principles determination of the enthalpy of formation of Mn–Si phases, Solid State Commun. 188 (2014) 49–52, http://dx.doi.org/10.1016/j.ssc.2014.02.021.
[7] C. Zeng, S.C. Erwin, L.C. Feldman, A.P. Li, R. Jin, Y. Song, J.R. Thompson, H.H. Weitering, Epitaxial ferromagnetic Mn_5Ge_3 on Ge(111), Appl. Phys. Lett. 83 (24) (2003) 5002–5004, http://dx.doi.org/10.1063/1.1633684.
[8] M. Petit, L. Michez, C.-E. Dutoit, S. Bertaina, V.O. Dolocan, V. Heresanu, M. Stoffel, V. Le Thanh, Very low-temperature epitaxial growth of Mn_5Ge_3 and $Mn_5Ge_3C_{0.2}$ films on Ge(111) using molecular beam epitaxy, Thin Solid Films 589 (2015) 427–432, http://dx.doi.org/10.1016/j.tsf.2015.05.068.
[9] I. Kounta, H. Reichlova, D. Kriegner, R. Lopes Seeger, A. Bad'ura, M. Leiviska, A. Boussadi, V. Heresanu, S. Bertaina, M. Petit, E. Schmoranzerova, L. Smejkal, J. Sinova, T. Jungwirth, V. Baltz, S.T.B. Goennenwein, L. Michez, Competitive actions of MnSi in the epitaxial growth of Mn_5Si_3 thin films on Si(111), Phys. Rev. Mater. 7 (2023) 024416, http://dx.doi.org/10.1103/PhysRevMaterials.7.024416.
[10] Y. Tawara, K. Sato, On the magnetic anisotropy of single crystal of Mn_5Ge_3, J. Phys. Soc. Japan 18 (6) (1963) 773–777, http://dx.doi.org/10.1143/JPSJ.18.773.
[11] P.J. Brown, J.B. Forsyth, V. Nunez, F. Tasset, The low-temperature antiferromagnetic structure of Mn_5Si_3 revised in the light of neutron polarimetry, J. Phys.: Condens. Matter 4 (49) (1992) 10025, http://dx.doi.org/10.1088/0953-8984/4/49/029.
[12] P.J. Brown, J.B. Forsyth, Antiferromagnetism in Mn_5Si_3: the magnetic structure of the AF2 phase at 70 K, J. Phys.: Condens. Matter 7 (39) (1995) 7619, http://dx.doi.org/10.1088/0953-8984/7/39/004.
[13] N. Biniskos, F.J. dos Santos, K. Schmalzl, S. Raymond, M. dos Santos Dias, J. Persson, N. Marzari, S. Blügel, S. Lounis, T. Brückel, Complex magnetic structure and spin waves of the noncollinear antiferromagnet Mn_5Si_3, Phys. Rev. B 105 (2022) 104404, http://dx.doi.org/10.1103/PhysRevB.105.104404.
[14] L.-A. Michez, A. Spiesser, M. Petit, S. Bertaina, J.-F. Jacquot, D. Dufeu, C. Coudreau, M. Jamet, V.L. Thanh, Magnetic reversal in Mn_5Ge_3 thin films: an extensive study, J. Phys.: Condens. Matter 27 (26) (2015) 266001, http://dx.doi.org/10.1088/0953-8984/27/26/266001.
[15] T. Toliński, K. Synoradzki, Specific heat and magnetocaloric effect of the Mn_5Ge_3 ferromagnet, Intermetallics 47 (2014) 1–5, http://dx.doi.org/10.1016/j.intermet.2013.12.005.
[16] M. Gottschilch, O. Gourdon, J. Persson, C. de la Cruz, V. Petricek, T. Brueckel, Study of the antiferromagnetism of Mn5Si3: an inverse magnetocaloric effect material, J. Mater. Chem. 22 (2012) 15275–15284, http://dx.doi.org/10.1039/C2JM00154C.
[17] K. Kanematsu, Convalent bond and spin scheme in the intermetallic compound with $B8_2$ type, J. Phys. Soc. Japan 17 (1) (1962) 85–93, http://dx.doi.org/10.1143/JPSJ.17.85.
[18] G. Kappel, G. Fischer, A. Jaéglé, Magnetic investigation of the system Mn_5Ge_3-Mn_5Si_3, Phys. Status Solidi (a) 34 (2) (1976) 691–696, http://dx.doi.org/10.1002/pssa.2210340233.
[19] A. Berche, E. Théron-Ruiz, J.-C. Tédenac, P. Jund, Thermodynamic study of the Ge–Mn–Si system, J. Alloys Compd. 632 (2015) 10–16, http://dx.doi.org/10.1016/j.jallcom.2015.01.072.
[20] K. Vancon, Etude des silicogermaniures de manganese cristallisant dans la structure D88, C. R. Hebd. Seances Acad. Sci. 260 (1) (1965) 111.
[21] R. Haug, G. Kappel, A. Jaéglé, Electrical resistivity studies of the system Mn_5Ge_3-Mn_5Si_3, Phys. Status Solidi (a) 55 (1) (1979) 285–290, http://dx.doi.org/10.1002/pssa.2210550132.

[22] F. Zhao, W. Dagula, O. Tegus, K. Buschow, Magnetic-entropy change in $Mn_5Ge_{3-x}Si_x$ alloys, J. Alloys Compd. 416 (1) (2006) 43–45, http://dx.doi.org/10.1016/j.jallcom.2005.08.039.

[23] B. Siberchicot, R. Henrion, J. Toboła, Theoretical study of substitution of Si for Ge in Mn_5Ge_3, Acta Phys. Polon. A 91 (2) (1997) 467–470.

[24] K. Momma, F. Izumi, VESTA3 for three-dimensional visualization of crystal, volumetric and morphology data, J. Appl. Crystallogr. 44 (6) (2011) 1272–1276, http://dx.doi.org/10.1107/S0021889811038970.

[25] S. Olive-Mendez, A. Spiesser, L. Michez, V. Le Thanh, A. Glachant, J. Derrien, T. Devillers, A. Barski, M. Jamet, Epitaxial growth of Mn_5Ge_3/Ge(111) heterostructures for spin injection, Thin Solid Films 517 (1) (2008) 191–196, http://dx.doi.org/10.1016/j.tsf.2008.08.090, Fifth International Conference on Silicon Epitaxy and Heterostructures (ICSI-5).

[26] C. Zeng, W. Zhu, S.C. Erwin, Z. Zhang, H.H. Weitering, Initial stages of Mn adsorption on Ge(111), Phys. Rev. B 70 (2004) 205340, http://dx.doi.org/10.1103/PhysRevB.70.205340.

[27] M.G. Lagally, D.E. Savage, M.C. Tringides, Diffraction from Disordered Surfaces: An Overview, Springer US, Boston, MA, 1988, pp. 139–174, http://dx.doi.org/10.1007/978-1-4684-5580-911.

[28] J. Chevrier, V.L. Thanh, R. Buys, J. Derrien, A RHEED study of epitaxial growth of iron on a silicon surface: Experimental evidence for kinetic roughening, Europhys. Lett. 16 (8) (1991) 737, http://dx.doi.org/10.1209/0295-5075/16/8/006.

[29] P. De Padova, J.-M. Mariot, L. Favre, I. Berbezier, B. Olivieri, P. Perfetti, C. Quaresima, C. Ottaviani, A. Taleb-Ibrahimi, P. Le Fèvre, F. Bertran, O. Heckmann, M. Richter, W. Ndiaye, F. D'Orazio, F. Lucari, C. Cacho, K. Hricovini, Mn_5Ge_3 films grown on Ge(111)-c(2×8), Surf. Sci. 605 (5) (2011) 638–643, http://dx.doi.org/10.1016/j.susc.2011.01.002.

[30] M. Petit, A. Boussadi, V. Heresanu, A. Ranguis, L. Michez, Step flow growth of Mn_5Ge_3 films on Ge(111) at room temperature, Appl. Surf. Sci. 480 (2019) 529–536, http://dx.doi.org/10.1016/j.apsusc.2019.01.164.

[31] E. Arras, Étude Théorique De La Structure Et De La Stabilité Des Alliages GeMn Dans Le Cadre De La Spintronique. Un Prototype De Semiconducteur Magnétique Confronté Aux Résultats Expérimentaux (Ph.D. thesis), Université Joseph-Fourier - Grenoble I, 2010, URL https://theses.hal.science/tel-00489879.

[32] M.-A. Guerboukha, M. Petit, A. Spiesser, A. Portavoce, O. Abbes, V. Heresanu, S. Bertaina, C. Coudreau, L. Michez, Tuning the Mn_5Ge_3 and $Mn_{11}Ge_8$ thin films phase formation on Ge(111) via growth process, Thin Solid Films 761 (2022) 139523, http://dx.doi.org/10.1016/j.tsf.2022.139523.

[33] A.A. Stekolnikov, J. Furthmüller, F. Bechstedt, Absolute surface energies of group-IV semiconductors: Dependence on orientation and reconstruction, Phys. Rev. B 65 (2002) 115318, http://dx.doi.org/10.1103/PhysRevB.65.115318.

[34] P. Marée, K. Nakagawa, F. Mulders, J. van der Veen, K. Kavanagh, Thin epitaxial Ge-Si(111) films: Study and control of morphology, Surf. Sci. 191 (3) (1987) 305–328, http://dx.doi.org/10.1016/S0039-6028(87)81180-9.

[35] R. Zhachuk, J. Coutinho, Mechanisms of Si and Ge diffusion on surfactant terminated (111) silicon and germanium surfaces, Surf. Sci. 647 (2016) 12–16, http://dx.doi.org/10.1016/j.susc.2015.11.014.

[36] A. Portavoce, O. Abbes, Y. Rudzevich, L. Chow, V. Le Thanh, C. Girardeaux, Manganese diffusion in monocrystalline germanium, Scr. Mater. 67 (3) (2012) 269–272, http://dx.doi.org/10.1016/j.scriptamat.2012.04.038.

[37] O. Abbes, F. Xu, A. Portavoce, C. Girardeaux, K. Hoummada, V. Le Thanh, Effect of Mn Thickness on the Mn-Ge Phase Formation during Reactions of 50 nm and 210 nm Thick Mn Films Deposited on Ge(111) Substrate, in: Diffusion in Materials - DIMAT 2011, in: Defect and Diffusion Forum, vol. 323, Trans Tech Publications Ltd, 2012, pp. 439–444, http://dx.doi.org/10.4028/www.scientific.net/DDF.323-325.439.

[38] M.D. Kuzmin, Shape of temperature dependence of spontaneous magnetization of ferromagnets: Quantitative analysis, Phys. Rev. Lett. 94 (2005) 107204, http://dx.doi.org/10.1103/PhysRevLett.94.107204.

[39] İ. Gündüz Aykaç, M. Gülgün, Effect of Ge layer thickness on the formation of Mn_5Ge_3 thin film on Ge/Si(111), J. Magn. Magn. Mater. 473 (2019) 348–354, http://dx.doi.org/10.1016/j.jmmm.2018.10.096.